

1 Causes and consequences of pronounced variation in the 2 isotope composition of plant xylem water

3 Hannes P.T. De Deurwaerder ^{(1,2)*}, Marco D. Visser ⁽²⁾, Matteo Detto ⁽²⁾, Pascal Boeckx ⁽³⁾,
4 Félicien Meunier ^(1,4), Kathrin Kuehnhammer ^(5,6), Ruth-Kristina Magh ^(7,8), John D. Marshall
5 ⁽⁸⁾, Lixin Wang ⁽⁹⁾, Liangju Zhao ^(10,11), Hans Verbeeck ⁽¹⁾

6 (1) CAVElab - Computational & Applied Vegetation Ecology, Faculty of Bioscience Engineering, Ghent
7 University, Ghent, Belgium

8 (2) Department of Ecology and Evolutionary Biology, Princeton University, Princeton, NJ, USA

9 (3) ISOFYS – Isotope Bioscience Laboratory, Faculty of Bioscience Engineering, Ghent University, Ghent,
10 Belgium

11 (4) Ecological Forecasting Lab, Department of Earth and Environment, Boston University, Boston,
12 Massachusetts, USA

13 (5) IGOE, Umweltgeochemie, Technische Universität Braunschweig, Braunschweig, Germany

14 (6) Ecosystem Physiology, University of Freiburg, Freiburg, Germany,

15 (7) Institute for Forest Sciences, Chair of Tree Physiology, University of Freiburg, Freiburg, Germany

16 (8) Department of Forest Ecology and Management, SLU, Swedish University of Agricultural Sciences,
17 Umeå, Sweden

18 (9) Department of Earth Sciences, Indiana University-Purdue University Indianapolis (IUPUI),
19 Indianapolis, IN 46202, USA

20 (10) Shaanxi Key Laboratory of Earth Surface System and Environmental Carrying Capacity, College of
21 Urban and Environmental Sciences, Northwest University, Xi'an 710127, China

22 (11) Key Laboratory of Ecohydrology and Integrated River Basin Science, Northwest Institute of Eco-
23 Environment and Resources, Chinese Academy of Sciences, Lanzhou 730000, China

24

25 **Correspondence to:* Hannes De Deurwaerder (Hannes_de_deurwaerder@hotmail.com)

26

27

28 **Abstract**

- 29 1. Stable isotopologues of water are widely used to derive root water uptake (RWU)
30 profiles and average RWU depth in lignified plants. Uniform isotope composition of
31 plant xylem water (δ_{xyl}) along the stem length of woody plants is a central assumption
32 within the isotope tracing approach, which has never been properly evaluated.
- 33 2. Here we evaluate whether strong variation in δ_{xyl} within woody plants exists using
34 empirical field observations from French Guiana, northwestern China, and Germany. In
35 addition, supported by a mechanistic plant hydraulic model, we develop hypotheses on
36 how variation in δ_{xyl} can form through the effects of diurnal variation in RWU, sap flux
37 density, diffusion, and various other soil and plant parameters on the δ_{xyl} of woody
38 plants.
- 39 3. The hydrogen and oxygen isotope composition of plant xylem water shows strong
40 temporal (i.e., sub-daily) and spatial (i.e., along the stem) variation ranging up to 25.2‰
41 and 6.8‰ for $\delta^2\text{H}$ and $\delta^{18}\text{O}$ respectively, greatly exceeding measurement error range in
42 all evaluated datasets. Model explorations predict that significant δ_{xyl} variation could
43 arise from diurnal RWU fluctuations and vertical soil water heterogeneity. Moreover,
44 significant differences in δ_{xyl} emerge between individuals with different sap flux
45 densities.
- 46 4. This work shows a complex pattern of δ_{xyl} transport in the soil-root-xylem system, which
47 can be related to the dynamics of RWU by plants. These dynamics complicate the
48 assessment of RWU when using stable water isotopologues, but also open new
49 opportunities to study drought responses to environmental drivers. We propose to
50 include monitoring of sap flow and soil matric potential for more robust estimates of

51 average RWU depth and expansion of attainable insights in plant drought strategies and
52 responses.

53

54 **Keywords**

55 Deuterium, Ecohydrology, Lianas, Root water uptake, Sap flow, Stable isotope composition of
56 water, Tropical trees, Water competition

57

58 **1. Introduction**

59 The use of stable isotope composition of water has strengthened ecohydrology studies by
60 providing insights into phenomena that are otherwise challenging to observe, such as root water
61 uptake depth (RWU depth) (Rothfuss & Javaux, 2017), below-ground water competition and
62 hydraulic lift (Hervé-Fernández *et al.*, 2016; Meunier *et al.*, 2017). Compared to root
63 excavation, the technique is far less destructive and labor-intensive. This makes it more flexible
64 for studying multiple individuals across spatial and temporal scales (i.e. individual to
65 ecosystem, daily to seasonal) (Dawson *et al.* 2002). Besides, the study of stable isotope
66 composition of xylem water measures the real effects of RWU at different depths whereas
67 excavation yields only root distribution and architecture. The advantages and wide applicability
68 of this method make it a popular technique that pushes the boundaries of ecohydrology (Dawson
69 *et al.*, 2002; Yang *et al.*, 2010; Rothfuss & Javaux, 2017).

70 A variety of methods are used to infer average RWU depth from the isotope composition
71 of plant xylem water (δ_{xyl}), but all rely on a direct relationship between the isotopic compositions
72 of plant xylem and soil water (Ehleringer & Dawson, 1992). All have two key assumptions.
73 The first is that the isotope composition of plant xylem water remains unchanged during
74 transport from root uptake to evaporative sites (e.g. leaves and non-lignified green branches).
75 Hence, isotopic fractionation – i.e. processes that cause a shift in the relative abundances of the
76 water isotopologues, driven by their differences in molecular mass – do not occur during the
77 transport from the uptake to the evaporative site (Wershaw *et al.*, 1966; Zimmermann *et al.*,
78 1967; White *et al.*, 1985; Dawson & Ehleringer, 1991; Walker & Richardson, 1991; Dawson *et*
79 *al.*, 2002; Zhao *et al.*, 2016). Second, all methods assume that xylem water provides a well-
80 mixed isotope composition of water from different soil layers: sampled xylem water
81 instantaneously reflects the distribution and water uptake of the roots independent of the timing
82 or height of sampling.

83 The first assumption is relatively well supported. Isotopic fractionation at root level does
84 not raise concerns for most RWU assessments using water isotopologues (Rothfuss & Javaux,
85 2017) except for kinetic fractionation that might occur during water transported across the root
86 membrane in extreme environments (Lin & Sternberg, 1993; Ellsworth and Williams, 2007;
87 Zhao *et al.*, 2016). Similarly, isotopic fractionation of water within an individual plant, although
88 possible, is generally not considered a serious problem (Yakir, 1992; Dawson & Ehleringer,
89 1993; Cernusak *et al.*, 2005; Mamonov *et al.*, 2007; Zhao *et al.*, 2016). This perception was
90 recently contested by Barbeta *et al* (2020), advocating a more general nature of the occurrence
91 of isotopic offsets between xylem water and potential water sources. As the origin of these
92 offsets remains debated, future research should clarify its impact on the applicability of stable
93 water isotopic compositions for RWU assessment. However, the second assumption of time
94 and space invariance of the isotope composition of xylem water has, to our knowledge, never
95 been assessed.

96 Various plant physiological processes, ranging from very simple to more complex
97 mechanisms, could influence within plant variation in δ_{xyl} at short time scales, i.e. sub-daily to
98 sub-hourly. For instance, plant transpiration during the day is regulated by stomata according
99 to water supply and atmospheric demand, and follows well known diurnal patterns (Steppe &
100 Lemeur, 2004; Epila *et al.*, 2017). This results in a changing water potential gradient between
101 soil and leaves throughout the day (Fig 1a,b), which in turn affects the depth of the average
102 RWU (Goldstein *et al.*, 1998; Doussan *et al.*, 2006; Huang *et al.*, 2017). Hence, shifts in a
103 plant's capacity to take up water at different soil layers during the day can generate diurnal
104 variation in the mixture of isotope composition from water taken up from various depths (Fig
105 1c). Subsequently, this water mixture moves up along the xylem with the velocity of the sap
106 flux density. As these sap flux densities depend on species and individual-specific hydraulic
107 traits and their responses to atmospheric water demand and soil moisture availability, complex

108 dynamics in isotopic composition will emerge and propagate through the plant. The above
109 hypothesis, if true, would make the comparison of isotopic data among individuals, species,
110 and studies difficult.

111 In this study, we provide a critical assessment of the assumption of δ_{xyl} invariance along
112 the length of woody plant stems and over short time periods. We first show that variation in δ_{xyl}
113 along the length of lignified plants exceeds the expected measurement error using three
114 independent datasets including i) canopy trees and lianas sampled at different heights in French
115 Guiana; and ii) plant species from northwestern China (Zhao *et al.*, 2014) and iii) European
116 Beech and Silver firs in south-west Germany (Magh *et al.*, 2020). Second, we build a simple
117 mechanistic model that incorporates basic plant hydraulic transport processes. The model
118 predicts that diurnal changes in water potential gradient between soil and roots result in shifting
119 sources of water absorption that differ in their isotope composition.

120

121 **2. Materials and Methods**

122 **2.1. Part A: Empirical exploration**

123 **2.1.1. Field data French Guiana: variation in δ_{xyl} with plant height**

124 Six canopy trees and six canopy lianas were sampled during two subsequent dry days (24-25
125 August 2017) at the Laussat Conservation Area in Northwestern French Guiana (05°28.604'N-
126 053°34.250'W). Stem xylem tissue of individual plants was sampled at different heights (1.3,
127 5, 10, 15 and 20 m where possible) at the same radial position of the stem, between 9:00 and
128 15:00. Stem samples were stripped off bark and phloem tissues. Soil samples were collected at
129 different depths (0.05, 0.15, 0.30, 0.45, 0.60, 0.90, 1.20, and 1.80m) with a soil auger and in
130 close vicinity to the sampled individuals. Samples were placed in glass collection vials, sealed
131 with a cap and frozen awaiting cryogenic vacuum distillation (CVD; 4 h at 105°C). When the

132 weight loss of a sample resulting from the extraction process was below 98%, the sample was
133 excluded (after Araguás-Araguás *et al.*, 1998) (see Fig S1).

134 The isotope composition of the water in the samples was measured with a Wavelength-
135 Scanned-Cavity Ring-Down Spectrometer (WS-CRDS, L2120-i, Picarro, California, USA)
136 coupled with a vaporizing module (A0211 High Precision Vaporizer) and a micro combustion
137 module to avoid organic contamination (Martin-Gomez *et al.*, 2015; Evaristo *et al.*, 2016). Post-
138 processing of raw δ -readings into calibrated δ -values (in ‰, v-smow) was performed using
139 SICalib (version 2.16; Gröning, 2011). More details on the sampling site and sampling
140 procedure can be found in supplementary methods A.

141 **2.1.2. Field data China: temporal variation in δ_{xyt}**

142 Plant δ_{xyt} was sampled at high temporal resolution in the Heihe River Basin (HRB),
143 northwestern China during field campaigns described in Zhao *et al.* (2014). Four distinct study
144 locations differing in altitude, climatological conditions, and ecosystem types were selected. At
145 each location, the dominant tree, shrub, and/or herb species were considered for sampling. In
146 August 2009, *Populus euphratica* was sampled in the Qidaoqiao riparian forest (42°01'N-
147 101°14'E) and *Reaumuria soongorica* in the Gobi desert ecosystem (42°16'N-101°17'E; 906-
148 930 m a.s.l). In June–September 2011 *Picea crassifolia*, *Potentilla fruticose*, *Polygonum*
149 *viviparum* and *Stipa capillata* were measured in the Pailugou forest ecosystem (38°33'N-
150 100°18'E; 2700-2900 m a.s.l). All species were sampled every 2-hours over multiple days (3-
151 4), except for *P. crassifolia* which was measured hourly. Stem samples were collected for trees
152 and shrubs, while root samples were obtained for the herb species. More details are available
153 in Zhao *et al.* (2014)).

154 Upon collection, all samples were placed in 8 mL collection bottles and frozen in the
155 field stations before transportation to the laboratory for water extraction via CVD (Zhao *et al.*,

156 2011). Both $\delta^{18}O$ and δ^2H were assessed with an Euro EA3000 element analyzer (Eurovector,
157 Milan, Italy) coupled to an Isoprime isotope ratio mass spectrometer (Isoprime Ltd, UK) at the
158 Heihe Key Laboratory of Ecohydrology and River Basin Science, Cold and Arid Regions
159 Environmental and Engineering Research Institute. Internal laboratory references were used for
160 calibration, resulting in measurement precision of $\pm 0.2\text{‰}$ and $\pm 1.0\text{‰}$ for $\delta^{18}O$ and δ^2H ,
161 respectively.

162 **2.1.3. Field data Germany: high temporal variation in δ_{xyl}**

163 Magh *et al.* (2020) conducted an extensive δ_{xyl} monitoring campaign (6-11 July 2017) studying
164 mature Silver firs (*Abies alba*; n=3) and European beeches (*Fagus sylvatica*; n=3) during
165 progressing drought conditions, at the “Freiamt” field site in south-west Germany. Isotopic
166 composition of xylem water was obtained from branch samples, which were collected every
167 two hours between 7:00 and 21:00 at the same height and canopy orientation in the sun crown.
168 Branches were stripped of bark and phloem tissue. A Scholander Pressure chamber
169 (Scholander, 1966), which allowed concomitant registration of water potential of the sampled
170 branches, was used to extract xylem water directly in the field (Rennenberg *et al.*, 1996). Both
171 $\delta^{18}O$ and δ^2H of branch samples were determined with a wavelength scanned cavity ring-down
172 spectrometer (Picarro L2130i, Santa Clara, USA), followed by data correction using
173 ChemCorrect™ (Picarro, 2010). For more details see Magh *et al.* (2020).

174

175 **2.1.4. Field data normalization**

176 To aid visual comparisons, we use normalized δ_{xyl} – values (β^2H_X and $\beta^{18}O_X$) which describe
177 the deviation of an individual sample from the average isotopic composition (a) along the height
178 h of the stem, or (b) over one day:

$$179 \quad \beta^2H_X = \delta^2H_X - \frac{1}{N} \sum_{j=1}^N \delta^2H_{X,j} \quad \text{Eq. (1)}$$

180 With N the number of sampled heights or time steps during one day.

181

182 **2.2. Part B: Model exploration**

183 **2.2.1. Model derivation**

184 The expected δ_{xyl} at different stem heights within a tree during the course of the day can be
185 derived from plant and physical properties such as root length density, total fine root surface
186 area, water potential gradients, and the isotope composition of soil water (Fig. 2). We call this
187 the SWIFT model (i.e. Stable Water Isotopic Fluctuation within Trees). To derive the SWIFT
188 model, we first describe the establishment of δ_{xyl} entering the tree at the stem base via a multi-
189 source mixing model (Phillips & Gregg, 2003). We subsequently consider vertical water
190 transport within the tree, which relates to the established sap flow pattern.

191 To ensure consistency and clarity in variable declarations we maintain the following
192 notation in the subscripts of variables: uppercase roman to distinguish the medium through
193 which water travels (X for xylem, R for root, S for soil) and lowercase for units of time and
194 distance (h for stem height, t for time and i for soil layer index). A comprehensive list of
195 variables, definitions, and units is given in Table 1. A schematic representation of the model is
196 provided in Fig. 2a. Note that the model presented here focuses on hydrogen isotopes (i.e.
197 $^2\text{H}/^1\text{H}$) but can easily be used to study oxygen isotopes (i.e. $^{18}\text{O}/^{16}\text{O}$).

198 *i. Isotope composition of plant xylem water at stem base.*

199 The $\delta^2\text{H}$ composition of xylem water of an individual plant at stem base ($\delta^2H_{X,0,t}$) (i.e.
200 height zero; $h = 0\text{m}$; Fig. 2a) at time t , can theoretically be derived by calculating a weighted
201 average of water taken up from different soil depths (Phillips & Gregg, 2003). The root zone
202 is divided into n discrete soil layers of equivalent thickness Δz . Here, we assume a constant $\delta^2\text{H}$
203 composition of soil water ($\delta^2H_{S,i}$) over time in each soil layer, a reasonable assumption when

204 isotopic measurements are conducted during rain-free periods, allowing the expression of
 205 $\delta^2H_{X,0,t}$ as:

$$206 \quad \delta^2H_{X,0,t} = \sum_{i=1}^n f_{i,t} \cdot \delta^2H_{S,i} \quad \text{Eq. (2)}$$

207 where $f_{i,t}$ is the fraction of water taken up at the i^{th} soil layer (Fig. 2a) defined as:

$$208 \quad f_{i,t} = \frac{RWU_{i,t}}{\sum_{i=1}^n RWU_{i,t}} \quad \text{Eq. (3)}$$

209 and $RWU_{i,t}$ is the net amount of water entering and leaving the roots at time t in the i^{th} soil layer
 210 ($RWU_{i,t}$ is defined positive when entering the root). The current representation of the model
 211 does not account for water loss via the root system nor for mixing of the extracted water from
 212 different soil layers within the roots until the water enters the stem base. When tree capacitance
 213 is neglected, the sum of $RWU_{i,t}$ across the entire root zone is equal to the instantaneous sap
 214 flow at time t , SF_t :

$$215 \quad SF_t = \sum_{i=1}^n RWU_{i,t} = \sum_{i=1}^n -k_i \cdot A_{R,i} \cdot [\Psi_{X,0,t} - (\Psi_{S,i,t} - z_i)] \quad \text{Eq. (4)}$$

216 Where k_i is the plant-specific total soil-to-root conductance over soil layer i , $\Psi_{X,0,t}$ is the water
 217 potential (i.e. the hydraulic head) at the base of the plant stem and $\Psi_{S,i,t}$ is the soil matric
 218 potential at the i^{th} soil layer (Fig. 2a). Total plant water potential is generally defined as the sum
 219 of the solute, pressure, gravity, and matric potential. As long-distance water transport through
 220 the xylem is studied, the osmotic potential and the kinetic energy head can be assumed
 221 negligible (Früh & Kurth, 1999). The xylem pressure potential is represented as $\Psi_{X,0,t}$. And the
 222 term z_i is the gravimetric water potential necessary to lift the water from depth z_i to the base of
 223 the stem, assuming a hydrostatic gradient in the transporting roots. The model considers z_i to
 224 be a positive value (zero at the surface), thus z_i is subtracted $\Psi_{S,i,t}$. $A_{R,i}$ is the absorptive root
 225 area distribution over soil layer i (Fig. 2a). This parameter $A_{R,i}$ can be derived from plant

226 allometric relations with stem diameter (Čermák *et al.*, 2006), and subsequently distributed over
 227 the different soil layers, considering the power-law distribution of Jackson *et al.* (1995).

228 The total soil-to-root conductance is calculated assuming the root and soil resistances are
 229 connected in series (Fig. 2a):

$$230 \quad k_i = \frac{k_R \cdot k_S}{k_R + k_S} \quad \text{Eq. (5)}$$

231 where k_R is the effective root radial conductivity (assumed constant and uniform), and $k_S =$
 232 $K_{S,i}/\ell$ is the conductance associated with the radial water flow between soil and root surface.
 233 $\ell = 0.53/\sqrt{\pi \cdot B_i}$ represents the effective radial pathway length of water flow between bulk soil
 234 and root surface (De Jong van Lier *et al.*, 2008; Vogel *et al.*, 2013) with B_i giving the overall
 235 root length density distribution per unit of soil. $K_{S,i}$ is the soil hydraulic conductivity for each
 236 soil depth. $K_{S,i}$ depends on soil water moisture and thus relates to the soil matric potential $\Psi_{S,i,t}$
 237 of the soil layer where the water is extracted. $K_{S,i}$ is computed using the Clapp & Hornberger
 238 (1978) formulation:

$$239 \quad K_{S,i} = K_{S,max} \cdot \left(\frac{\Psi_{sat}}{\Psi_{S,i,t}} \right)^{2+\frac{3}{b}} \quad \text{Eq. (6)}$$

240 where $K_{S,max}$ is the soil conductivity at saturation and b and Ψ_{sat} are empirical constants that
 241 depend on soil type (here considered as constant over all soil layers).

242 Subsequently, $f_{i,t}$ can be restructured as:

$$243 \quad f_{i,t} = \frac{k_i \cdot A_{R,i} \cdot \Delta\Psi_{i,t}}{\sum_{i=1}^n k_i \cdot A_{R,i} \cdot \Delta\Psi_{i,t}} \quad \text{Eq. (7)}$$

244 where the root water to soil matric potential gradient is represented as $\Delta\Psi_{i,t} = \Psi_{X,0,t} -$
 245 $(\Psi_{S,i,t} - z_i)$.

246 Combining Eq. (2) and Eq. (7) then allows the derivation of $\delta^2 H_{X,0,t}$ as follows:

247
$$\delta^2 H_{X,0,t} = \sum_{i=1}^n \left(\frac{k_i \cdot A_{R,i} \cdot \Delta \Psi_{i,t}}{\sum_{j=1}^n k_j \cdot A_{R,j} \cdot \Delta \Psi_{j,t}} \cdot \delta^2 H_{S,i} \right)$$
 Eq. (8)

248 This equation requires estimates of $\Delta \Psi_{i,t}$, which is preferably measured instantaneously in the
 249 field (i.e. via stem and soil psychrometers for $\Psi_{X,0,t}$ and $\Psi_{S,i,t}$, respectively). However, as
 250 measurements of $\Psi_{X,0,t}$ are not always available, estimated $\hat{\Psi}_{X,0,t}$ can be derived from sap flow
 251 by re-organizing Eq. (4) into:

252
$$\hat{\Psi}_{X,0,t} = \frac{\sum_{i=1}^n [k_i \cdot A_{R,i} \cdot (\Psi_{S,i,t} - z_i)] - SF_t}{\sum_{i=1}^n k_i \cdot A_{R,i}}$$
 Eq. (9)

253 which then allows replacement of $\Psi_{X,0,t}$ with $\hat{\Psi}_{X,0,t}$ in Eq. (8).

254 *ii. Height-dependent isotope composition of plant xylem water*

255 In our model, the water isotopologues simply move upwards from the stem base with
 256 the sap flow velocity. Assuming negligible diffusion, the $\delta^2\text{H}$ isotope composition in xylem
 257 water at height h and time t ($\delta^2 H_{X,h,t}$) is then the isotope composition of xylem water at stem
 258 base at time $t - \tau$.

259
$$\delta^2 H_{X,h,t} = \delta^2 H_{X,0,t-\tau}$$
 Eq. (10)

260 where τ is the lag before $\delta^2 H_{X,0,t}$ reaches stem height h (Fig. 2a), which depends on the true
 261 sap flux density in the xylem (SF_V). True sap flux density indicates the real speed of vertical
 262 water displacement within a plant, derived by dividing SF_t over the lumen area of the plant (A_x ;
 263 Fig. 2a) i.e. the total cross-sectional area of the vessels. τ can be obtained from the mass
 264 conservation equality:

265
$$h \cdot A_x = \int_{t-\tau}^t SF_t dt$$
 Eq. (11)

266 Note that since most scientific studies express sap flux density as the sap flow over the total
267 sapwood area (SF_S), rather than over the total vessel lumen area (SF_V), for consistency, we will
268 present the model outputs as functions of SF_S .

269 Note that SF_V presents the sap flux density normalized over the total vessel lumen area, and
270 as vessel lumen area correlates with plant diameter at breast height (DBH), there is no need for
271 explicit consideration of DBH in the model for comparison among field measurements.

272 Model analyses show that the impact of the mutual diffusion coefficient of heavy water in
273 normal water on the transport flux is negligible for plants with high sap flux densities, which is
274 the case for the theoretical examples below. However, in plants with low sap flow densities,
275 consideration of diffusion might be required. Diffusion might also be generated by water
276 passing through a complex network of vessels, in analogy to diffusion in a porous media (see
277 supplementary methods B for some analytical results, simulated cases of and a detailed
278 discussion on the role of diffusion). SWIFT was implemented in R version 3.4.0 (R Core Team,
279 2017), and is publicly available (see GitHub repository HannesDeDeurwaerder/SWIFT).

280 *iii. Model parameterization and analyses*

281 The model's primary purpose is to gain insight into 1) which processes are capable of
282 generating $\delta_{xy|}$ variance, and 2) how sensitive the variance in $\delta_{xy|}$ along the stem is in response
283 to the modeled plant hydraulic processes. To this end, we adopted the basic plant parameters
284 from Huang *et al.* (2017) who studied soil-plant hydrodynamics of loblolly pine (*Pinus taeda*
285 *L.*) during a 30-day extended dry down period (Table S1). We started with synthetic basal sap
286 flow patterns and volumes extracted from the model runs of Huang *et al.* (2017) for a typical
287 drought day (day 11). Both basal sap flow patterns and volumes are repeated over the studied
288 period, as no variation between days is assumed. Sap flow follows the plant's water demand
289 which is the result of daily cycles of transpiration driven by photosynthetic active solar radiation

290 (PAR), vapor pressure deficit (VPD), and optimal stomatal response (Epila *et al.*, 2017).
291 Secondly, both the soil matric potential ($\Psi_{S,i,t}$) and $\delta^2\text{H}$ composition of soil water ($\delta^2H_{S,i}$)
292 profiles with soil depth were adopted from Meißner *et al.* (2012) (Fig. S8, see Table S1 for
293 equations) as driver data of the model, and were assumed to stay constant over time. Since
294 measurements of Meißner *et al.* (2012) were conducted at a silt loam plot in the temperate
295 climate of central Germany, corresponding soil parameters were selected from Clapp &
296 Hornberger (1978). Subsequently, the following model simulations were executed (see Fig. 2a):

- 297 1) **Analysis A1: impact of temporal SF_t variation on the isotope composition of**
298 **xylem water at a fixed stem height.** Temporal patterns in $\delta^2\text{H}$ isotope composition
299 in xylem water (δ^2H_X) were evaluated for a typical situation, i.e. measurement at
300 breast height ($h=1.30$ m) (e.g. White *et al.*, 1985; Meinzer *et al.*, 1999; Goldsmith
301 *et al.*, 2012; Hervé-Fernández *et al.*, 2016; De Deurwaerder *et al.*, 2018; Muñoz-
302 Villers *et al.*, 2019).
- 303 2) **Analysis A2: impact of temporal SF_t variation at different tree heights.**
304 Temporal patterns in δ^2H_X within a tree at various sampling heights (5, 10, and 15
305 m).
- 306 3) **Analysis A3: impact of temporal SF_t variation on the isotope composition of**
307 **xylem water and the timing of sampling.** Representation of the profile of δ^2H_X
308 along the full height of a tree, measured at different sampling times (9:00 and 11:00),
309 with the standard parameterization given in Table S1.
- 310 4) **Analysis B: variation in δ^2H_X due to differences in absolute daily average sap**
311 **flow speed.** Diurnal patterns in the δ^2H_X in trees that differ solely in daily averaged
312 SF_V , which are set to 0.64, 0.42, and 0.19 m h^{-1} (respectively corresponding to SF_S
313 values of 0.09, 0.06 and 0.03 m h^{-1}).

314 All parameters of the four analyses are given in Table S1. The model simulations
315 for each analysis were compared to a null model.

316

317 *iv. The null model*

318 The null model adopts the standard assumption of zero variation in δ_{xyl} along the length
319 of the plant body, but allows for potential measurement errors related to the extraction protocol.
320 In reality, empirically obtained data will have some variation as observed values (*Obs.* δ_{xyl})
321 are the sum of the true δ_{xyl} -values and their extraction error (*error*_{extraction}).

$$322 \quad \text{Obs. } \delta_{xyl} = \text{True } \delta_{xyl} + \text{error}_{\text{extraction}} \quad (\text{eq. 12})$$

323 Hence, the null model attributes any variance in isotopic composition to extraction errors, with
324 maximum extraction error ranges of 3‰ for δ^2H samples (0.3‰ for $\delta^{18}O$) expected for water
325 extraction recovery rates higher than 98% (e.g. Orłowski *et al.*, 2013). These extraction errors
326 are negatively skewed following the Rayleigh distillation model, which predicts that extraction
327 error for incomplete water recovery will be negative, and therefore $\text{Obs. } \delta_{xyl} \leq \text{True } \delta_{xyl}$. The
328 null model represents this *error*_{extraction} by a negative skew-normal distribution (with location
329 parameter $\zeta = 0\text{‰}$, the scale $\omega = 3\text{‰}$ for δ^2H or 0.3‰ for $\delta^{18}O$, and shape $\alpha = -\infty$) (Azzalini,
330 2013).

331

332 **2.2.2. Estimation of average RWU depth**

333 Average RWU depths (i.e. the weighted mean of the depths of RWU, with the uptake fractions
334 at the different depths as weights) were derived from the simulated δ^2H_x values by use of both
335 the direct inference method and the end-member mixing analysis method. Together, these
336 techniques represent 96% of the applied methods in the literature (Rothfuss & Javaux, 2017),
337 and the reader is referred to Rothfuss & Javaux (2017) for a complete discussion of both

338 techniques. In line with the general approach assessing RWU with stable water isotopes, the
339 average RWU depth is obtained by relating the δ^2H_X with the $\delta^2H_{S,i}$ depth profile. We
340 compared average RWU depth estimates obtained from simulated δ^2H_X , as described in the
341 analyses above, with the true average RWU depth. Here, the true average RWU depth was
342 defined as the depth corresponding to the daily weighted average δ^2H_X , calculated as the
343 weighted sum of $\delta^2H_{X,i,t}$ and the relative fraction of water taken up at each depth.

344

345 **2.2.3. Transport dynamics and sensitivity analysis**

346 We perform a basic model validation of our model assumption that the propagation of an
347 isotopic signature is driven by diurnal sap flow dynamics and diffusion alone. In essence, the
348 model assumes that once water with a given isotopic signature enters the stem, it moves
349 upwards with the speed of sap flow, and changes only due to the effect of diffusion. The effects
350 of capacitance on δ^2H_X dynamics by the release of storage water in the xylem flow can be
351 ignored. To validate this assumption we compare model predictions against observed δ^2H_X
352 dynamics monitored within a pine tree (*Pinus pinea* L.) following 2H -enrichment in a controlled
353 greenhouse experiment, as detailed in Marshall *et al.* (2020). δ^2H_X was measured at two heights
354 (0.15 and 0.65m) using a novel *in situ* technique, the borehole equilibration method. Performed
355 model simulations consider the absolute ranges of sap flux densities during the entire
356 monitoring campaign, with the account of tree tapering effect on sap flux densities over the
357 studied stem length (supplementary method C). Validation of diurnal variation in δ^2H_X requires
358 high temporal resolution monitoring of δ^2H_X dynamics in plants stems, with simultaneous high
359 temporal resolution monitoring and characterization of sap flow, soil water potential, and
360 isotopic composition. Such data does not yet exist to our best of knowledge.

361 In addition, we performed two sensitivity analyses to assess the relative importance of each
362 parameter in generating variance in δ^2H_X along the length of a plant. In both sensitivity analyses,

363 we varied model parameters one-at-a-time to assess the local sensitivity of the model outputs
364 for soil type, sap flux density, root properties, and sampling strategies. The sensitivity analysis
365 provides insight into possibilities for improving the design of field protocols, by revealing
366 potential key measurements and caveats in field setups. More details on the performed
367 sensitivity analysis and validation of transport dynamics are available in supplementary method
368 C.

369

370 **3. Results**

371 **3.1. Part A: Empirical exploration**

372 The null model assumes constant isotopic composition of root water uptake, with only limited
373 variance in isotopic composition introduced by extraction errors ($\beta^2H_X < 3\text{‰}$; $\delta^{18}O_X < 0.3\text{‰}$).
374 However, pronounced δ^2H_X variance within individual plants, exceeding the null model ranges,
375 are observed in all three independent datasets. The normalized δ^2H composition in xylem water
376 (β^2H_X) along the stem length of lianas and trees in French Guiana exceeded the null model by
377 a factor of 3.2 and 4.3, respectively (Fig. 3c, Fig. S2). Differences up to 13.1‰ and 18.3‰ in
378 δ^2H and 1.3‰ and 2.2‰ in $\delta^{18}O$ were observed in individuals of trees and lianas, respectively
379 (Supplementary method A, table A.).

380 Similarly, diurnal intra-individual δ^2H_X variances were found for all considered plant
381 growth forms, i.e. trees, shrubs, and herbs, monitored in China (Fig. 4b-d, Fig S3). Observed
382 daily maximum differences in δ^2H_X were 18.0‰, 21.0‰, and 25.2‰ for trees, shrubs and herbs
383 respectively (2.8‰, 6.8‰, and 6.5‰ in $\delta^{18}O_X$ in Fig. S4). The expected null model variance
384 was exceeded for each species during its measurement period.

385 Finally, pronounced intra-individual δ^2H_X variance was also observed for all monitored
386 firs and beeches in Germany (Fig 4e, Fig. S5). Here, daily maxima differences in δ^2H_X were 8.2

387 ‰ and 14.2 ‰ for *Abies alba* and *Fagus sylvatica* respectively (2.0‰ and 4.2 ‰ in $\delta^{18}O_X$ in
388 Fig. S6).

389

390 **3.2. Part B: Model exploration**

391 *Isotope composition of xylem water at stem base and basic model behavior*

392 At the stem base, simulated $\delta^2H_{X,0,t}$ displays a diurnal fluctuation (Fig. 2b, Fig S7) that
393 corresponds to the daily sap flow pattern (Fig. S7). This pattern is caused by shifting diurnal
394 average RWU depth. Early in the morning, when transpiration is low, most of the RWU occurs
395 in deeper layers, where soil matric potential is less negative and where soil water is more
396 depleted in δ^2H in comparison with the soil layers above (Fig. S8a-b). As transpiration increases
397 during the day, a significant proportion of RWU can now be extracted from the drier, shallower
398 layers, where the δ^2H -composition of soil water is enriched, hence higher. In the afternoon, as
399 transpiration declines, the isotopic composition reflects again the composition of the more
400 depleted soil water in the deeper soil layers, and it remains constant throughout the night
401 because apart from diffusion SWIFT does not consider mixing of the internal stem water. The
402 mixing effects of diffusion are only noticeable at low sap flow speeds (fig 3b).

403 The most enriched δ^2H_X -values (approx. -59‰) are found in alignment with the diurnal
404 minimum of $\Psi_{X,0,t}$ (approx. -0.85 MPa, Fig. S7). At this moment, the difference between $\Psi_{X,0,t}$
405 and $\Psi_{S,i,t}$ is maximal, enabling water extraction from the upper and driest soil layers. Most root
406 biomass is located near the surface (cf. Jackson *et al.*, 1995; Fig. S8c) and uptake in these layers
407 will result in relatively high contributions to the total RWU.

408 In contrast, differences between $\Psi_{X,0,t}$ and $\Psi_{S,i,t}$ are smaller in the early morning and
409 late afternoon causing root water uptake in the upper soil layers to halt. The decreasing in
410 absolute range of $\Delta\Psi_{i,t}$ translates into higher proportions of RWU originating from deeper, more

411 depleted soil layers. This causes δ^2H_X to drop to a baseline of approx. -67‰. This afternoon
412 depletion of δ^2H_X will henceforth be referred to as the δ^2H_X -baseline drop.

413 *Isotope composition of xylem water at different times, heights and SF_V*

414 Temporal fluctuation in δ^2H_X within a tree at 1.3 m (i.e. the standard sampling height;
415 Analysis A1; Fig. 2a) and other potential sampling heights (e.g. branch collection; Analysis A2;
416 Fig. 2a), are provided in Fig. 2b and 3a. Both analyses show that fluctuations in δ^2H_X depend
417 on the height of measurement and the corresponding time needed to move the water along the
418 xylem conduits. Note that it depends on the selected temporal resolution whether the δ^2H_X -
419 baseline drop at a given height equals the (stem base) minimum (here 1 min, see Fig. S12). In
420 addition to sampling height, analysis A3 depicts the importance of sampling time (Fig. 3a).
421 Outputs of analysis B predict that the occurrence and width of the δ^2H_X -baseline drop are a
422 function of the sap flow velocity SF_V (Fig. 3b). To aid model interpretation and comparability
423 with field data, we (i) provide an illustrative example of normalized δ^2H isotope composition
424 of model-simulated xylem water (β^2H_X) with consideration of extraction error (Fig. 4a), and (ii)
425 display the relation between δ^2H_X variance and cumulative sap flow volumes, for which the
426 piston flow dynamics in SWIFT originate from lateral translation of the δ^2H_X fluctuation at
427 $\delta^2H_{X,0,t}$ (Fig. 2b).

428

429 **3.2.1. Potential biases in average RWU depth estimation**

430 Both timing of measurement (Fig. 5a) and SF_V (Fig. 5b) influence average RWU depth
431 estimates derived via the direct inference and end-member mixing analysis method (Fig. S9).
432 Collection of tree samples at 1.30 m can result in erroneous estimation, deviating up to 104 %
433 from the average daily RWU depth (Fig. 5). Plotting the relative error in average RWU depth
434 as a function of time and SF_V (Fig. 5) shows that it is possible to time δ^2H_X measurements in a

435 fashion that captures unbiased estimates of the average RWU depth. Xylem water sampling
436 should be timed to capture the δ^2H_X that corresponds to water extracted at peak RWU, and the
437 expected sampling time can be derived by considering the time needed for the water to reach
438 the point of measurement (i.e. at 1.30 m in Fig. 5).

439

440 **3.2.2. Transport dynamics and sensitivity analysis**

441 Our sensitivity analyses show that the expected absolute error in average RWU depth
442 assessment is directly related to both 1) maximum variance in and 2) the probability of sampling
443 non-representative δ^2H_X values. The maximum variance depends on the height, while the
444 probability of sampling non-representative areas depends on the width of the “ δ^2H_X -baseline
445 drop” respectively (defined above). Hence, variation in δ^2H_X is determined by several factors,
446 including the sampling strategy (timing and height of sampling), sap flow velocity (Fig. S10),
447 and below-ground biophysical parameter (Fig. S11). We summarized the most important
448 variables as predicted by SWIFT, which should be considered in subsequent RWU studies.

449 Plants on loamy soils show larger diurnal δ^2H_X variances in comparison with those on clay
450 soils for a similar prevailing isotope gradient across the soil profile. Larger variances
451 correspond to potentially larger errors, but the steeper slope of the δ^2H_X curve results in a thinner
452 δ^2H_X -baseline drop. Hence, loamy soil can result in potentially the large error but this is
453 mediated by a lower probability of sampling non-representative δ^2H_X values during the day.

454 The volume of water taken up by the plant (SF_t ; Fig. S11b) affects xylem water potential
455 of the plant at stem base ($\hat{\Psi}_{X,0,t}$). Higher SF_t requires more negative $\hat{\Psi}_{X,0,t}$, enabling the plant
456 to access more shallow and enriched soil layers. Therefore, an increase in SF_t results in the
457 increase of maximum δ^2H_X values (increased maximum error) but also results in a smaller width

458 of the baseline drop (Fig. 2-3). Lower SF_t result in smaller errors, but a larger probability of
459 sampling a non-representative area (Fig. 3b).

460 Root properties, i.e. root membrane permeability (Fig. S11c) strongly influence both the
461 total range of δ^2H_X variance and the width of the δ^2H_X -baseline drops. Decreasing root
462 membrane permeability, but with no alterations to the sap flow volumes, results in thinner δ^2H_X -
463 baseline drops, but higher maximum δ^2H_X variance.

464 In addition, the true sap flow velocity (SF_t per unit of lumen area) will determine the relative
465 importance of diffusion on the δ^2H_X dynamics. Diffusion can cause a smoothing of the peak and
466 a consequent increase in the width of the δ^2H_X -baseline drop. However, as diffusion is
467 proportional to the time the isotope remains in the xylem, its absolute impact on δ^2H_X is
468 negligible in plants with a high true sap flow velocity. In contrast, the impact of diffusion on
469 δ^2H_X dynamics is substantial for plants with very low velocities, where water takes many days
470 to pass from roots to leaves (see supplementary method B).

471 The role of diffusion was investigated using a stepwise δ^2H enrichment experiment in Marshall *et al.*
472 (2020) (Fig 6). Analytical solutions of an advection-diffusion equation show that at 0.15 cm, a relatively
473 small diffusivity was required to reproduce the initial increase of xylem isotope signature, with values
474 comparable to these reported for diffusivity of heavy water (Meng *et al.*, 2018). However, at 65 cm, the
475 value of diffusivity required to match the observed initial increase was much higher, suggesting other
476 processes besides molecular diffusivity might contribute to the isotope transport (e.g. variable flow
477 velocities within vessels and among vessels of the xylem network). Note also that the analytical solutions
478 were not able to recover the second part of the curve where the isotope reaches the asymptotic enriched
479 value, which is more gradual in the observations (Fig. 6). This also suggests a complex transport of δ^2H_X
480 in the xylem.

481

482 **4. Discussion**

483 **4.1. Dynamic diurnal isotope compositions of xylem water along plant stems**

484 Empirical field data show pronounced δ_{xyl} variance along the stem length (Fig. 3) and over a
485 sub-daily time period (Fig. 4). Our model explorations suggest that basic plant hydraulic
486 functioning can result in shifting mixtures of δ^2H_X entering the plant (Fig. 2-3). Daily $\Psi_{X,0,t}$
487 fluctuations interact with the $\Psi_{S,i,t}$ profile causing different parts of the root distribution to be
488 active during the day. The fluctuations in δ^2H_X at the stem base propagate along the xylem with
489 a velocity proportional to the sap flow and this produces variability in sampled δ^2H_X that is
490 much larger than the expected measuring error. Consequently, rather than being static, δ^2H_X
491 values along the height of a plant should be envisioned as a dynamic diurnal process.

492 Importantly, we show that high variance in δ^2H_X can result in an incorrect assessment
493 of differences in average RWU depths between plants. Differences do not necessarily result
494 from variability in average RWU depth, but may result from monitoring plants at different
495 heights (Fig. 2-3), at different times (Fig. 3a) or by comparing individuals which have different
496 SF_V (Fig. 3b) and xylem anatomical properties. For example, depending on SF_V and lumen area,
497 the isotopic signal can take hours or days to travel from roots to leaves - as was also observed
498 experimentally (Steppe *et al.*, 2010; Magh *et al.*, 2020; Marshall *et al.*, 2020).

499 Low SF_V allows multiple δ^2H_X -baseline drops over the length of a single tree. Sampled
500 δ^2H_X can reflect soil isotopic composition of the past several days. Our sensitivity analysis
501 reveals that various soil and plant characteristics have an important role in determining both the
502 daily maximum δ^2H_X variance as well as the width of the δ^2H_X -baseline drop. These two
503 characteristics directly impact (i) the expected maximum bias in estimates of average RWU
504 depth and (ii) the chance of measuring δ^2H_X values that do not represent a mixture of all rooting
505 layers during peak RWU (i.e. measurements in the baseline drop). Ultimately, these factors will
506 challenge the use of stable water isotope to study the terrestrial water fluxes as recently

507 reviewed by Penna *et al.* (2018). We additionally advocate that future research should explore
508 the minimum set of (bio)physiological drivers and processes that require quantification to
509 correctly interpret δ^2H_X along the hydraulic pathway length of a plant.

510

511 **4.2. General applicability of model and results**

512 A necessary condition for diurnal shifts in RWU is the existence of water potential differences,
513 e.g. more negative water potentials in the upper layers where trees usually have higher root
514 density, which can cause a disproportional partitioning of diurnal RWU between deep and
515 shallow roots over a diurnal course. The pronounced variance in δ_{xyl} identified in this study is
516 intrinsic to the isotopic tracing technique for RWU assessment, as this method relies on the
517 existence of a soil water isotopic profile. Such profiles are the result of soil evaporation, a
518 process inextricably coupled to water potential heterogeneity, and hence to variance in δ^2H_X .

519 Plant transpiration results from a complex interaction between atmospheric demands
520 (i.e. driven by VPD and radiation) and stomatal conductance that depends on tolerance for
521 drought stress and soil moisture content. We may expect diurnal fluctuation in radiation and
522 VPD, and hence in water transport and depth of water absorption, as modeled here to be a
523 general phenomenon in nature. Moreover, much greater fluctuations in VPD and radiation
524 should be expected under natural conditions than the diurnal cycle described here, and these
525 will increase the variability of transpiration fluxes, leading to even more complex dynamics of
526 $\Psi_{X,0,t}$. Specifically, the model simulations suggest that intra-individual variability of δ^2H_X will
527 reflect the past changes of RWU dynamics, including RWU dynamics driven by changes of
528 environmental demands. For instance, a changing degree in cloud cover that impacts sap flow
529 dynamics can influence $\Psi_{X,0,t}$ rather abruptly (e.g. in lianas; Chen *et al.*, 2015) and lead to

530 instantaneous changes in the δ^2H composition of the water mixture taken up at the root level.
531 This can complicate the comparison of different plants sampled at different heights and times.

532 Note that, based on our model, we expect that soil isotopic enrichment experiments will
533 generate extensive δ^2H_X variation along the length of trees whenever diurnal RWU fluctuations
534 cause water extraction to shift between labeled and unlabeled soil layers. Furthermore, when
535 enrichment experiments target trees with different hydraulic properties (such as SF_V) care
536 should be taken to determine when and where to sample these trees to assess an enriched isotope
537 composition (Fig 6, but see Magh *et al.*, 2020;).

538

539 **4.3. Alternative causes of δ_{xyl} fluctuation.**

540 The SWIFT model provides a simple traceable and mechanistic explanation, using diurnal
541 variations in SF_t and RWU, for the pronounced variance and dynamic nature of the δ_{xyl}
542 fluctuations with plant height and time of field samples (e.g. Fig. 3-4) and elsewhere (Cooper
543 *et al.* 1991). However, several other processes might contribute to generate variability, while
544 others can act to damp this variability. In the next section, we will discuss alternative causes,
545 complementary and antagonistic, that contribute to the observed intra-individual δ_{xyl} variances.

546 *i. Fractionation at root or stem level*

547 An increasing body of observations shows the occurrence of isotopic fractionation at the
548 root level governed by root membrane transport (Lin & Sternberg, 1993; Vargas *et al.*, 2017)
549 or by unknown reasons (Zhao *et al.*, 2016). Brinkmann *et al.* (2019) hypothesize that root level
550 fractionation causes disparity when average RWU depth calculations based on δ^2H_X
551 measurements are compared with those of $\delta^{18}O_X$. However, it is difficult to imagine a scenario
552 where root fractionation by itself can explain the observed diurnal fluctuations in δ_{xyl} with
553 height and time. Even if root fractionation significantly contributed to variation in δ_{xyl} , we

554 would still need to take into account diurnal fluctuation in RWU to explain the observed
555 patterns. Isotopic enrichment of xylem water along the stem length was observed in association
556 with stem transpiration (Dawson & Ehleringer, 1993; Barnard *et al.*, 2006). However, this
557 phenomenon is generally restricted to non-suberized plants and in woody branches in close
558 vicinity to the evaporative surface of the plant (Dawson & Ehleringer, 1993). Isotopic
559 enrichment can, therefore, not explain the variances in δ_{xyl} observed in our empirical data, which
560 were sampled within the main stem (data French Guiana) or from lignified branch segment
561 distant from evaporative surfaces (data China and Germany).

562 ii. *Temporal and spatial soil dynamics*

563 Soil water content can be extremely heterogeneous in the three spatial dimensions as well
564 as in time with complex dynamics of soil water movement. For example, hydraulic lift vertically
565 redistributes soil water through the roots (Dawson & Ehleringer, 1993), which may change the
566 water isotopic composition of the water mixture in the rhizosphere that is taken up by roots.
567 Specifically, hydraulic lift redistributes and mixes the depleted isotopic signal of deeper layers
568 with the enriched signal in the rhizosphere in shallower layers. This should lead to lower
569 variation in the soil water accessible to the plant, and hence less variation along plant height.
570 Horizontal heterogeneity of water content may also affect δ_{xyl} variance as soil water potentials
571 and the isotope composition of soil water are interlinked. Under these conditions, it is important
572 to understand how much the radial distribution of roots will naturally average out soil
573 heterogeneity. However, note that heterogeneity in the soil does not automatically translate in
574 variability in the xylem. Differential root water uptake driven by the diurnal fluctuation in water
575 potential gradients in the soil-plant interface is still required to generate variability in the xylem
576 isotopic signature.

577 iii. *Storage tissue and phloem enrichment*

578 Storage tissues release water and sugars into the xylem conduits on a daily basis to support
579 water transpiration demand (Goldstein et al., 1998; Morris et al., 2016; Secchi et al., 2017) or
580 to repair embolism (Salleo et al., 2009; Secchi et al., 2017). Both water and sugars are
581 transported in and out of storage tissue via symplastic pathways using plasmodesmata and
582 aquaporins (Knipfer et al., 2016; Secchi et al., 2017), a pathway that has been linked to isotopic
583 fractionation in roots (Ellsworth & Williams, 2007). Moreover, phloem transports
584 photosynthetic assimilates that were produced in the leaves and are therefore potentially
585 affected by transpiration fractionation (Gessler *et al.*, 2013). Hence, these metabolic molecules
586 might show higher values of δ^2H and $\delta^{18}O$ compared to RWU. Water release from storage or
587 phloem tissue might locally alter δ_{xyl} (White et al., 1985). Additionally, the time between water
588 storage and release could bridge multiple days, and corresponding isotopic composition may
589 reflect soil conditions antecedent a dry spell when the isotopic signature of soil was less
590 vertically stratified. It is evident that such dynamics are complex, and it is hard to predict how
591 storage tissue and phloem enrichment affect observed δ_{xyl} patterns. Importantly, xylem isotopic
592 sampling cannot differentiate between water resulting from RWU or storage, and therefore we
593 cannot exclude the possibility that tissue and phloem enrichment play a role. At a minimum this
594 adds further uncertainty to RWU assessment. Water derived from storage tissues might also be
595 present in larger fraction in higher parts of the plants, especially branches, as contamination
596 accumulates as water moves upwards.

597 Unfortunately, to our best knowledge, empirical data on the isotopic composition of storage
598 tissue and its spatiotemporal dynamics are absent in the literature. Future research should target
599 impact assessment of storage water on intra-individual δ_{xyl} , allowing proper implementation in
600 the model.

601 *Diffusion processes*

602 Diffusion is a process of net movement of molecules from a region of higher concentration
603 to a region of lower concentration. Consequently, diffusion dampens δ_{xyl} variability, both in
604 time and space within water xylem. Although the mutual diffusion coefficient of heavy water
605 in normal water is very small and flow within vessels is laminar, other processes might still
606 contribute to generating diffusion along the xylem. For example, as the water moves through
607 the complex network of vessels, differences in velocities between vessels of different sizes
608 cause some particles to move faster or slower than average flow. According to the Hagen–
609 Poiseuille law, the flow in each vessel is proportional to the fourth power of the vessel radius
610 and the mean velocity to the square of the radius, thus potentially generating large differences
611 in particle velocities depending on the vessel size distribution and other anatomical properties.
612 Even within a single vessel, velocity is parabolic with a maximum flow velocity in the center
613 and zero at the vessel walls.

614 **4.4. A way forward**

615 The observed large δ_{xyl} variance and temporal dynamics in the empirical data suggest
616 the need for a critical assessment of the stable isotope tracer technique for RWU studies.
617 However, it also creates new opportunities. Since δ_{xyl} variance and temporal dynamics herein
618 likely relate to various plant physiological processes, monitoring of variation in δ_{xyl} can allow
619 a more integrated understanding of plant water transport and hydraulic properties.

620 Combining a plant hydraulic model with *in situ* SF_V , $\delta^2H_{S,i}$ and $\Psi_{S,i,t}$ can also help
621 improve the robustness of RWU assessment and interpretation. Measurements of $\delta^2H_{S,i}$ and
622 $\Psi_{S,i,t}$ at multiple depths, i.e. by installing soil water suction cups working at a vacuum (i.e.
623 Rennenberg *et al.*, 1996) and multiple soil matric potential sensors that measure at a high
624 temporal frequency, should be especially valuable since the SWIFT model showed high
625 sensitivity to alterations of this variable and these can be directly supplied as model inputs. At

626 the same time, the availability of SF_t measurements allows for identifying the moment when
627 water uptake from all root layers is at its maximum, which can be used to determine the optimal
628 timing of sampling at a given height providing a more robust estimation of average RWU depth
629 and uptake.

630 Alongside the modeling approach presented here, new ways to study δ^2H_X at a high
631 temporal scale are strongly encouraged. For example, the pioneering work of Volkmann *et al.*
632 (2016) to the development of an *in situ* continuous isotope measurement technique that offers
633 the possibility for monitoring δ_{xyl} at a sub-hourly resolution. This technique holds strong
634 promise for further elucidating the natural δ^2H_X variances found within plants and the
635 physiology processes from which these variances result. Such high temporal resolution of
636 isotope measurements, coupled with *in situ* monitoring of various environmental and plant
637 biophysical metrics, are needed for both model improvement and further validation. Moreover,
638 these seem inevitable to eventually differentiate all causal mechanisms of the observed intra-
639 individual δ_{xyl} variance.

640

641 **5. Conclusions**

642 A collection of empirical field data show pronounced variance and high temporal
643 fluctuations in δ_{xyl} . Moreover, these high temporal fluctuations in δ_{xyl} emanate from basic plant
644 hydraulic functioning as model explorations show. We expect the observed δ_{xyl} variance and
645 sub-daily fluctuations result, for a large part, from the mechanisms considered here, though
646 various other physiological processes could also affect δ_{xyl} .

647 Our theoretical explorations warn that variability in the isotope composition of plant
648 xylem water can result in erroneous average RWU depth estimation and will complicate the
649 interpretation and comparison of data: samples taken at different heights, times or plants

650 differing in SF_V may incorrectly show differences in average RWU depth. We further predict
651 that various soil parameters and plant hydraulic parameters affect (i) the absolute size of the
652 error and (ii) the probability of measuring δ_{xyl} values that do not represent the well-mixed values
653 during the plants' peak RWU. Hydraulic models, such as SWIFT, could help to design more
654 robust sampling regimes that enable improved comparisons between studied plants. We
655 advocate the addition of SF_t , which indirectly reflects diurnal RWU fluctuations, and $\Psi_{S,i,t}$
656 monitoring as a minimum in future RWU assessments since these parameters were predicted to
657 be the predominant factors introducing variance in δ_{xyl} from the SWIFT model exploration.
658 However, soil texture and root permeability are also key measurements especially when
659 comparing across species and sites.

660 Our findings do not exclude additional factors that impact the observed intra-individual
661 δ_{xyl} variance and temporal fluctuation as many processes can act simultaneously and are not
662 mutually exclusive. Therefore, we strongly emphasize the need for more research. Directed
663 studies that validate and quantify the relative impact of other plant physiological processes
664 towards variance in δ_{xyl} are a prerequisite before improved modeling tools can be developed.

665

666 **Acknowledgment**

667 This research was funded by the European Research Council Starting Grant 637643
668 (TREECLIMBERS), the FWO grants (1507818N, V401018N to HDD), the Carbon Mitigation
669 Initiative at Princeton University (MD, MDV), Agence Nationale de la Recherche
670 "Investissement d'Avenir" grant (CEBA: ANR-10-LABX-25-01), the Belgian American
671 Educational Foundation (BAEF to FM) and the WBI (FM). We are grateful to Samuel Bodé,
672 Megan Bartlett, Isabel Martinez Cano, and Pedro Hervé-Fernández who provided feedback on
673 analytical and interpretative aspects of the study. We thank Dries Van Der Heyden, Wim Van

674 Nunen, Laurence Stalmans, Oscar Vercleyen, Katja Van Nieuland, Stijn Vandevoorde, and
675 Clément Stahl for data collection and lab processing. We credit Pascal Petronelli and Bruce
676 Hoffman for species identification, and Cora N. Betsinger for proofreading. Cheng-Wei
677 Huang's work provided inspiration for this research.

678

679 **Author contribution**

680 H.V., M.D.V, and P.B. supervised and provided guidance throughout all aspects of the research.
681 H.D.D., M.D.V, and H.V. designed the study. H.D.D., K.K., R.K.M., J.D.M., L.W., and L.Z.
682 collected and processed the empirical datasets. The model was developed and coded by H.D.D,
683 M.D.V, M.D., and F.M. All authors contributed to the interpretation of the results and the text
684 of the manuscript.

685

686 **Data availability**

687 Both the French Guiana data and the SWIFT model are available on the GitHub repository
688 HannesDeDeurwaerder/SWIFT. For the availability of the data collected in China and
689 Germany, readers are referred to Zhao *et al.* (2014) and Magh *et al.* (2020) respectively.

690

691 **Competing interests**

692 The authors declare that they have no conflict of interest.

693

694 **References**

- 695 **Araguás- Araguás L, Froehlich K, Rozanski K. 1998.** Stable isotope composition of
696 precipitation over southeast Asia. *Journal of Geophysical Research: Atmospheres* **103**:
697 28721–28742.
- 698 **Azzalini A. 2013.** *The skew-normal and related families*. Cambridge University Press.
- 699 **Barbeta A, Gimeno TE, Clavé L, Fréjaville B, Jones SP, Delvigne C, Wingate L, Ogée J.**
700 **2020.** An explanation for the isotopic offset between soil and stem water in a temperate tree
701 species. *New Phytologist*.
- 702 **Barnard RL, De Bello F, Gilgen AK, Buchmann N. 2006.** The $\delta^{18}\text{O}$ of root crown water
703 best reflects source water $\delta^{18}\text{O}$ in different types of herbaceous species, *Rapid Commun.*
704 *Mass Sp.*, 20, 3799–3802.
- 705 **Brinkmann N, Eugster W, Buchmann N, Kahmen A. 2019.** Species- specific differences
706 in water uptake depth of mature temperate trees vary with water availability in the soil. *Plant*
707 *Biology* **21**: 71–81.
- 708 **Čermák J, Ulrich R, Staněk Z, Koller J, Aubrecht L. 2006.** Electrical measurement of tree
709 root absorbing surfaces by the earth impedance method: 2. Verification based on allometric
710 relationships and root severing experiments. *Tree physiology* **26**: 1113–1121.
- 711 **Cernusak LA, Farquhar GD, Pate JS. 2005.** Environmental and physiological controls over
712 oxygen and carbon isotope composition of Tasmanian blue gum, *Eucalyptus globulus*. *Tree*
713 *physiology* **25**: 129–146.
- 714 **Chen Y, Cao K, Schnitzer SA, Fan Z, Zhang J, Bongers F, Chen Y. 2015.** Water-use
715 advantage for lianas over trees in tropical seasonal forests. : 128–136.
- 716 **Clapp RB, Hornberger GM. 1978.** Empirical equations for some soil hydraulic properties.
717 *Water resources research* **14**: 601–604.
- 718 **Cooper LW, DeNiro MJ, Keeley JE. 1991.** The relationship between stable oxygen and
719 hydrogen isotope ratios of water in stomatal plants.
- 720 **Dawson TE, Ehleringer JR. 1991.** Streamside trees that do not use stream water. *Nature*
721 **350**: 335–337.
- 722 **Dawson TE, Ehleringer JR. 1993.** Isotopic enrichment of water in the “woody” tissues of
723 plants: implications for plant water source, water uptake, and other studies which use the
724 stable isotopic composition of cellulose. *Geochimica et Cosmochimica Acta* **57**: 3487–3492.
- 725 **Dawson TE, Mambelli S, Plamboeck AH, Templer PH, Tu KP. 2002.** Stable isotopes in
726 plant ecology. *Annual review of ecology and systematics* **33**: 507–559.
- 727 **De Deurwaerder H, Hervé-Fernández P, Stahl C, Burban B, Petronelli P, Hoffman B,**
728 **Bonal D, Boeckx P, Verbeeck H. 2018.** Liana and tree below-ground water competition—
729 evidence for water resource partitioning during the dry season. *Tree Physiology*.

730 **Doussan C, Pierret A, Garrigues E, Pagès L. 2006.** Water uptake by plant roots: II–
731 modelling of water transfer in the soil root-system with explicit account of flow within the
732 root system—comparison with experiments. *Plant and soil* **283**: 99–117.

733 **Ehleringer JR, Dawson TE. 1992.** Water uptake by plants: perspectives from stable isotope
734 composition. *Plant, Cell & Environment* **15**: 1073–1082.

735 **Ellsworth PZ, Williams DG. 2007.** Hydrogen isotope fractionation during water uptake by
736 woody xerophytes. *Plant and Soil* **291**: 93–107.

737 **Epila J, Maes WH, Verbeeck H, Camp J Van, Okullo JBL, Steppe K. 2017.** Plant
738 measurements on African tropical *Maesopsis eminii* seedlings contradict pioneering water use
739 behaviour. *Environmental and Experimental Botany* **135**: 27–37.

740 **Früh T, Kurth W. 1999.** The hydraulic system of trees: theoretical framework and numerical
741 simulation. *Journal of theoretical Biology* **201**: 251–270.

742 **Gessler A, Brandes E, Keitel C, Boda S, Kayler ZE, Granier A, Barbour M, Farquhar
743 GD, Treydte K. 2013.** The oxygen isotope enrichment of leaf- exported assimilates—does it
744 always reflect lamina leaf water enrichment? *New Phytologist* **200**: 144–157.

745 **Goldsmith GR, Muñoz- Villers LE, Holwerda F, McDonnell JJ, Asbjornsen H, Dawson
746 TE. 2012.** Stable isotopes reveal linkages among ecohydrological processes in a seasonally
747 dry tropical montane cloud forest. *Ecohydrology* **5**: 779–790.

748 **Goldstein G, Andrade JL, Meinzer FC, Holbrook NM, Cavelier J, Jackson P, Celis A.
749 1998.** Stem water storage and diurnal patterns of water use in tropical forest canopy trees.
750 *Plant, Cell & Environment* **21**: 397–406.

751 **Hervé- Fernández P, Oyarzún C, Brumbt C, Huygens D, Bodé S, Verhoest NEC,
752 Boeckx P. 2016.** Assessing the ‘two water worlds’ hypothesis and water sources for native
753 and exotic evergreen species in south- central Chile. *Hydrological Processes* **30**: 4227–4241.

754 **Huang C, Domec J, Ward EJ, Duman T, Manoli G, Parolari AJ, Katul GG. 2017.** The
755 effect of plant water storage on water fluxes within the coupled soil–plant system. *New
756 Phytologist* **213**: 1093–1106.

757 **Jackson PC, Cavelier J, Goldstein G, Meinzer FC, Holbrook NM. 1995.** Partitioning of
758 water-resources among plants of a lowland tropical forest. *Oecologia* **101**: 197–203.

759 **De Jong van Lier Q, Van Dam JC, Metselaar K, De Jong R, Duijnsveld WHM. 2008.**
760 Macroscopic root water uptake distribution using a matric flux potential approach. *Vadose
761 Zone Journal* **7**: 1065–1078.

762 **Knipfer T, Cuneo I, Brodersen C, McElrone AJ. 2016.** In-situ visualization of the
763 dynamics in xylem embolism formation and removal in the absence of root pressure: a study
764 on excised grapevine stems. *Plant Physiology*: pp-00136.

765 **Lin G, Sternberg L. 1993.** Hydrogen isotopic fractionation by plant roots during water
766 uptake in coastal wetland plants. Stable isotopes and plant carbon-water relations. Elsevier,

767 497–510.

768 **Magh R-K, Eiferle C, Burzlaff T, Dannenmann M, Rennenberg H, Dubbert M. 2020.**
769 Competition for water rather than facilitation in mixed beech-fir forests after drying-wetting
770 cycle. *Journal of Hydrology*: 124944.

771 **Mamonov AB, Coalson RD, Zeidel ML, Mathai JC. 2007.** Water and deuterium oxide
772 permeability through aquaporin 1: MD predictions and experimental verification. *The Journal*
773 *of general physiology* **130**: 111–116.

774 **Marshall JD, Cuntz M, Beyer M, Dubbert M, Kuehnhammer K. 2020.** Borehole
775 equilibration: testing a new method to monitor the isotopic composition of tree xylem water in
776 situ. *Frontiers in Plant Science* **11**: 358.

777 **Meinzer FC, Andrade JL, Goldstein G, Holbrook NM, Cavelier J, Wright SJ. 1999.**
778 Partitioning of soil water among canopy trees in a seasonally dry tropical forest. *Oecologia*
779 **121**: 293–301.

780 **Meißner M, Köhler M, Schwendenmann L, Hölscher D. 2012.** Partitioning of soil water
781 among canopy trees during a soil desiccation period in a temperate mixed forest.
782 *Biogeosciences* **9**: 3465–3474.

783 **Meng W, Xia Y, Chen Y, Pu X. 2018.** Measuring the mutual diffusion coefficient of heavy
784 water in normal water using a double liquid-core cylindrical lens. *Scientific reports* **8**: 1–7.

785 **Meunier F, Rothfuss Y, Bariac T, Biron P, Richard P, Durand J-L, Couvreur V,**
786 **Vanderborght J, Javaux M. 2017.** Measuring and modeling hydraulic lift of *Lolium*
787 *multiflorum* using stable water isotopes. *Vadose Zone Journal*.

788 **Morris H, Plavcová L, Cvecko P, Fichtler E, Gillingham MAF, Martínez- Cabrera HI,**
789 **McGlenn DJ, Wheeler E, Zheng J, Ziemińska K. 2016.** A global analysis of parenchyma
790 tissue fractions in secondary xylem of seed plants. *New Phytologist* **209**: 1553–1565.

791 **Muñoz-Villers LE, Geris J, Alvarado-Barrientos S, Holwerda F, Dawson TE. 2019.**
792 Coffee and shade trees show complementary use of soil water in a traditional agroforestry
793 ecosystem. *Hydrology and Earth System Sciences Discussion*.

794 **Orlowski N, Frede HG, Brüggemann N, Breuer L. 2013.** Validation and application of a
795 cryogenic vacuum extraction system for soil and plant water extraction for isotope analysis. *J.*
796 *Sens. Sens. Syst* **2**: 179–193.

797 **Penna D, Hopp L, Scandellari F, Allen ST, Benettin P, Beyer M, Geris J, Klaus J,**
798 **Marshall JD, Schwendenmann L. 2018.** Ideas and perspectives: Tracing terrestrial
799 ecosystem water fluxes using hydrogen and oxygen stable isotopes—challenges and
800 opportunities from an interdisciplinary perspective. *Biogeosciences*.

801 **Phillips DL, Gregg JW. 2003.** Source partitioning using stable isotopes: coping with too
802 many sources. *Oecologia* **136**: 261–269.

803 **Rennenberg H, Schneider S, Weber P. 1996.** Analysis of uptake and allocation of nitrogen

804 and sulphur compounds by trees in the field. *Journal of Experimental Botany* **47**: 1491–1498.

805 **Rothfuss Y, Javaux M. 2017.** Reviews and syntheses: Isotopic approaches to quantify root
806 water uptake: a review and comparison of methods. *Biogeosciences* **14**: 2199.

807 **Salleo S, Trifilò P, Esposito S, Nardini A, Gullo MA Lo. 2009.** Starch-to-sugar conversion
808 in wood parenchyma of field-growing *Laurus nobilis* plants: a component of the signal
809 pathway for embolism repair? *Functional Plant Biology* **36**: 815–825.

810 **Scholander PF. 1966.** The role of solvent pressure in osmotic systems. *Proceedings of the*
811 *National Academy of Sciences of the United States of America* **55**: 1407.

812 **Secchi F, Pagliarani C, Zwieniecki MA. 2017.** The functional role of xylem parenchyma
813 cells and aquaporins during recovery from severe water stress. *Plant, cell & environment* **40**:
814 858–871.

815 **Steppe K, Lemeur R. 2004.** An experimental system for analysis of the dynamic sap-flow
816 characteristics in young trees: results of a beech tree. *Functional Plant Biology* **31**: 83–92.

817 **Steppe K, De Pauw DJW, Doody TM, Teskey RO. 2010.** A comparison of sap flux density
818 using thermal dissipation, heat pulse velocity and heat field deformation methods.
819 *Agricultural and Forest Meteorology* **150**: 1046–1056.

820 **Vargas AI, Schaffer B, Yuhong L, Sternberg L da SL. 2017.** Testing plant use of mobile
821 vs immobile soil water sources using stable isotope experiments. *New Phytologist* **215**: 582–
822 594.

823 **Vogel T, Dohnal M, Dusek J, Votrubova J, Tesar M. 2013.** Macroscopic modeling of plant
824 water uptake in a forest stand involving root-mediated soil water redistribution. *Vadose Zone*
825 *Journal* **12**.

826 **Volkman THM, Kühnhammer K, Herbstritt B, Gessler A, Weiler M. 2016.** A method
827 for in situ monitoring of the isotope composition of tree xylem water using laser spectroscopy.
828 *Plant, cell & environment* **39**: 2055–2063.

829 **Walker CD, Richardson SB. 1991.** The use of stable isotopes of water in characterizing the
830 source of water in vegetation. *Chemical Geology* **94**: 145–158.

831 **Wershaw RL, Friedman I, Heller SJ, Frank PA. 1966.** Hydrogen isotopic fractionation of
832 water passing through trees. *Advances in organic geochemistry*: 55.

833 **White JWC, Cook ER, Lawrence JR, Broecker WS. 1985.** The D/H ratios of sap in trees -
834 implications for water sources and tree-ring D/H ratios. *Geochimica et Cosmochimica Acta*
835 **49**: 237–246.

836 **De Wispelaere L, Bodé S, Hervé-Fernández P, Hemp A, Verschuren D, Boeckx P. 2016.**
837 Plant water resource partitioning and xylem-leaf deuterium enrichment in a seasonally dry
838 tropical climate. *Biogeosciences Discuss.* **2016**: 1–26.

839 **Yakir D. 1992.** Variations in the natural abundance of oxygen-18 and deuterium in plant
840 carbohydrates. *Plant, Cell & Environment* **15**: 1005–1020.

- 841 **Yang Q, Xiao H, Zhao L, Zhou M, Li C, Cao S. 2010.** Stable isotope techniques in plant
842 water sources: a review. *Sciences in Cold and Arid Regions* **2**: 112–122.
- 843 **Zhao L, Wang L, Cernusak LA, Liu X, Xiao H, Zhou M, Zhang S. 2016.** Significant
844 difference in hydrogen isotope composition between xylem and tissue water in *Populus*
845 *euphratica*. *Plant, Cell & Environment* **39**: 1848–1857.
- 846 **Zhao L, Wang L, Liu X, Xiao H, Ruan Y, Zhou M. 2014.** The patterns and implications of
847 diurnal variations in the d-excess of plant water, shallow soil water and air moisture.
- 848 **Zhao L, Xiao H, Zhou J, Wang L, Cheng G, Zhou M, Yin L, McCabe MF. 2011.** Detailed
849 assessment of isotope ratio infrared spectroscopy and isotope ratio mass spectrometry for the
850 stable isotope analysis of plant and soil waters. *Rapid Communications in Mass Spectrometry*
851 **25**: 3071–3082.
- 852 **Zimmermann U, Ehhalt D, Münnich K. 1967.** Soil-Water movement and
853 evapotranspiration: changes in the isotopic composition of the water. Conference on Isotopes
854 in Hydrology. Vienna, 567-585.
- 855
- 856

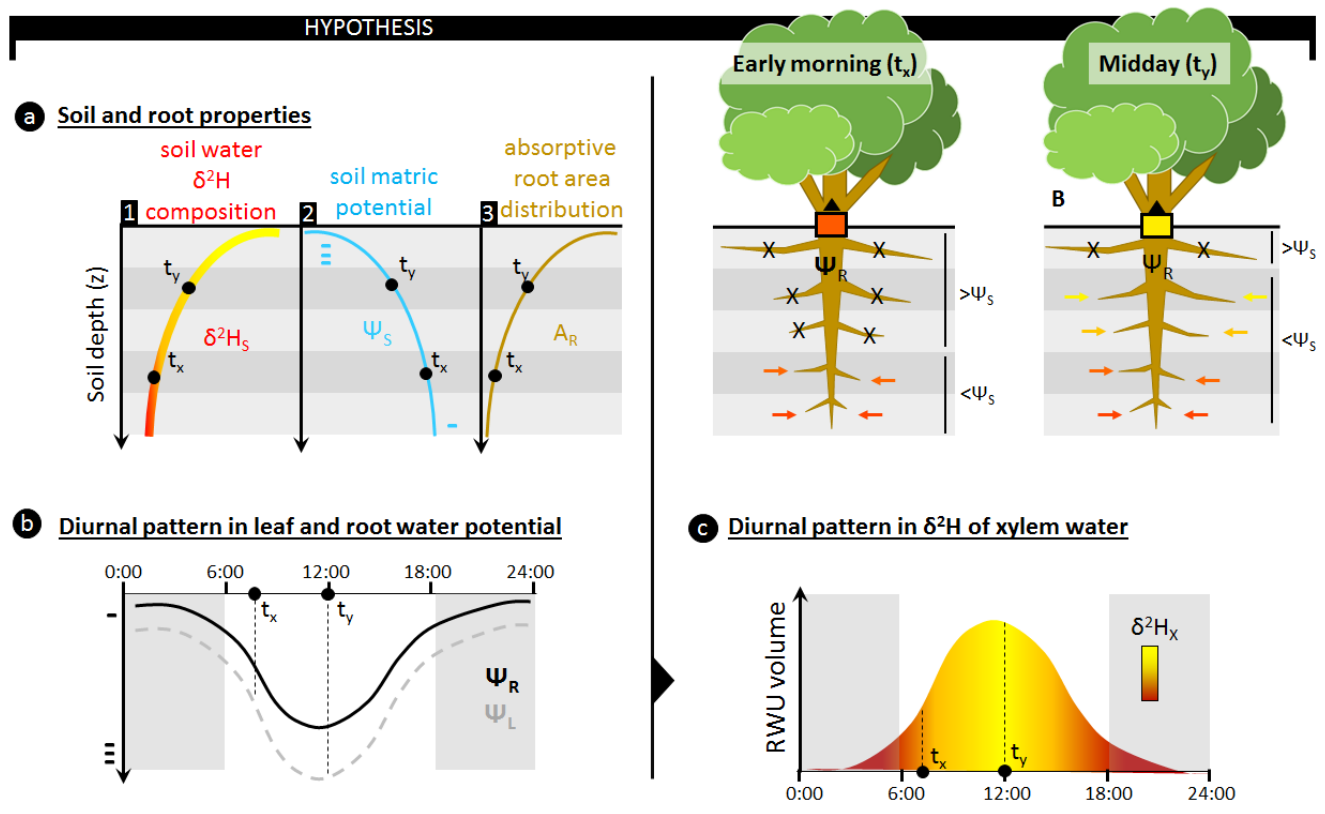
Symbol	Description	Unit
$A_{R,i}$	The absorptive root area distribution over soil layer i	m^2
A_{Rtot}	The plants' total active fine root surface area	m^2
$A_{SAPWOOD}$	Sapwood area	m^2
A_x	Total lumen area	m^2
b	Shape parameter for the soil hydraulic properties (Clapp & Hornberger, 1978)	dimensionless
B_i	The overall root length density distribution per unit of soil, not necessarily limited to the focal plant.	m m^{-3}
$\delta^2H_{X,0,t}$	Isotope composition of plant xylem water at stem base at time t	in ‰ VSMOW
$\delta^2H_{X,h,t}$	Isotope composition of plant xylem water at height h and time t	in ‰ VSMOW
$\delta^2H_{S,i}$	Isotope composition of soil water of the i^{th} soil layer (constant over time)	in ‰ VSMOW
δ_{sample}	Isotope composition of water within a sample	in ‰ VSMOW
$\Delta\hat{\Psi}_{i,t}$	Estimated water potential gradient between stem base and the i^{th} soil layer at time t derived from Eq. (8)	m
$\Delta\Psi_{i,t}$	Soil matric potential gradient between soil and roots at the i^{th} soil layer at time t	$\text{m H}_2\text{O}$
$\beta^2H_X; \beta^{18}O_X$	Normalized isotope composition of plant xylem water	in ‰ VSMOW
$f_{i,t}$	The fraction of water taken up in the i^{th} soil layer at time t	dimensionless
h	Measurement height	m
i	Soil layer index	dimensionless
δ_{xyl}	Isotope composition of plant xylem water	in ‰ VSMOW
k_i	Soil-root conductance of the i^{th} soil layer	s^{-1}
K_{max}	Maximum soil hydraulic conductivity	m s^{-1}
k_R	Effective root radial conductivity	s^{-1}
k_S	The conductance associated with the radial water flow between the soil and the root surface	s^{-1}
$K_{S,i}$	Soil hydraulic conductivity at the i^{th} soil layer	m s^{-1}
ℓ	The approximated radial pathway length of water flow between bulk soil and root surface	m
LF	Lumen fraction per unit sapwood area	$\text{m}^2 \text{m}^{-2}$
n	Number of unique contributing water sources	#
Ψ_{sat}	Soil matric potential at soil saturation	m
$\Psi_{S,i,t}$	Soil matric potential of the i^{th} soil layer at time t	m
$\Psi_{X,0,t}$	Water potential at the base of the plant stem at time t	m

R	Heavy to light isotope ratio measured in the sample or standard	%
$RWU_{i,t}$	Net amount of water entering and leaving the root tissues per unit of time in the i^{th} soil layer at time t	$\text{m}^3 \text{s}^{-1}$
SF_t	Instantaneous sap flow at time t	$\text{m}^3 \text{s}^{-1}$
SF_S	Sap flow velocity, calculated as the sap flow per sapwood area	m h^{-1}
SF_V	True sap flux density, calculated as the sap flow per lumen area	m h^{-1}
τ	Delay before the isotope composition of xylem water at stem base reaches stem height h	s
θ_{sat}	Soil moisture content at soil saturation	$\text{m}^3 \text{m}^{-3}$
$\theta_{S,i,t}$	Soil moisture content of the i^{th} soil layer at time t	$\text{m}^3 \text{m}^{-3}$
z_i	Soil depth of the i^{th} soil layer	m

859

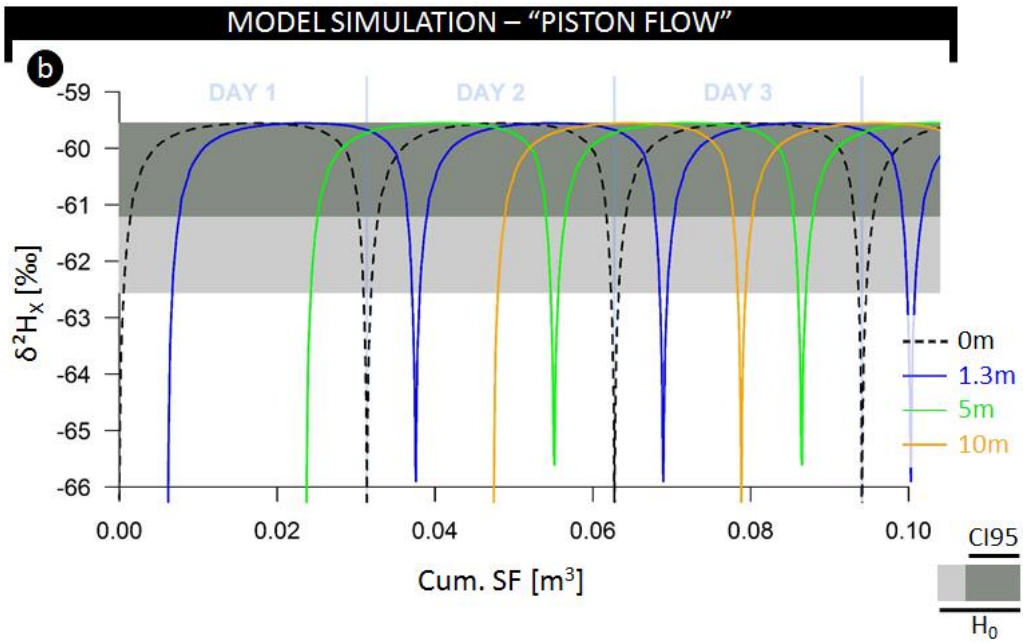
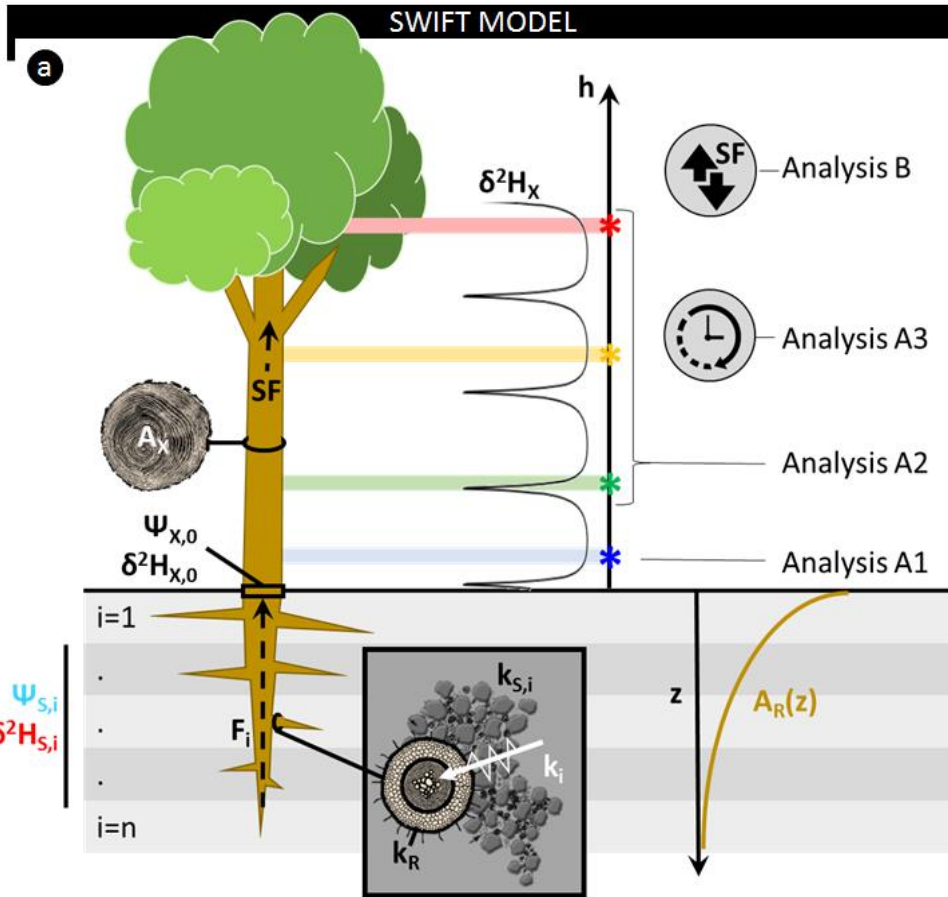
860

861



864
865 **Fig 1.** The use of stable water isotopes ($\delta^2\text{H}$ and $\delta^{18}\text{O}$) to assess the depth of root water uptake
866 (RWU) requires a depth gradient in isotopic composition of soil water ($\delta^2\text{H}_s$) to be present (**a,**
867 **line 1**), as only then can the relative contribution of different soil layers to the isotopic
868 composition in a plant's xylem water ($\delta^2\text{H}_x$) be derived. These $\delta^2\text{H}_s$ gradients occur naturally
869 as the result of evaporative soil drying during drought conditions, however, these conditions
870 also result in the formation of a gradient in soil matric potential (Ψ_s), ensuring an increasing Ψ_s
871 with depth (**a, line 2**). RWU and sap flow in plants are passive processes where water flows in
872 the direction of decreasing water potentials. Specifically for RWU, this implies that water influx
873 through the absorptive root area (A_R ; **a, line 3**) of a plant's root is facilitated whenever the water
874 potential in the root (Ψ_R) is more negative than the surrounding Ψ_s . As A_R and Ψ_s are generally
875 not uniform with soil depth (z), the relative contribution of a specific soil layer to RWU will
876 depend on (i) the difference between Ψ_s and Ψ_R in that soil layer, and (ii) the relative amount
877 of absorptive root area in that soil layer. Stable water isotopes techniques assume that the $\delta^2\text{H}_x$

878 reflects the contribution of δ^2H_S from all soil layers. However, this does not account for diurnal
879 fluctuations in Ψ_R which are invoked by the diurnal patterns in a plant's transpiratory water
880 demands (**panel b**). Typically, more negative Ψ_R values are observed when water demands are
881 high, i.e. around midday. However, a decrease in Ψ_R will result in higher RWU, and alter the
882 contribution of different soil layers to RWU. Specifically, dryer and shallower soil layers, with
883 more negative Ψ_S , could start contributing to RWU as Ψ_R decreases (**panel c**). For example, in
884 the early morning (situation t_x) when Ψ_R is high, only deeper soil layers where $\Psi_S > \Psi_R$
885 contribute to overall δ^2H composition of the RWU flux. As Ψ_L and Ψ_R decrease towards midday
886 (situation t_y) more water can be absorbed from shallower soil layers. As the A_R in these shallow
887 soil layers is high, they strongly affect the relative contribution of δ^2H_S entering the plant.
888 Hence, diurnal fluctuations in Ψ_R will result in fluctuating mixtures of δ^2H_S entering the plant.
889 As these δ^2H_S mixtures are transported along the xylem pathway, they produce variance in δ^2H_X ,
890 which could complicate RWU assessments via stable water isotope analysis.



891

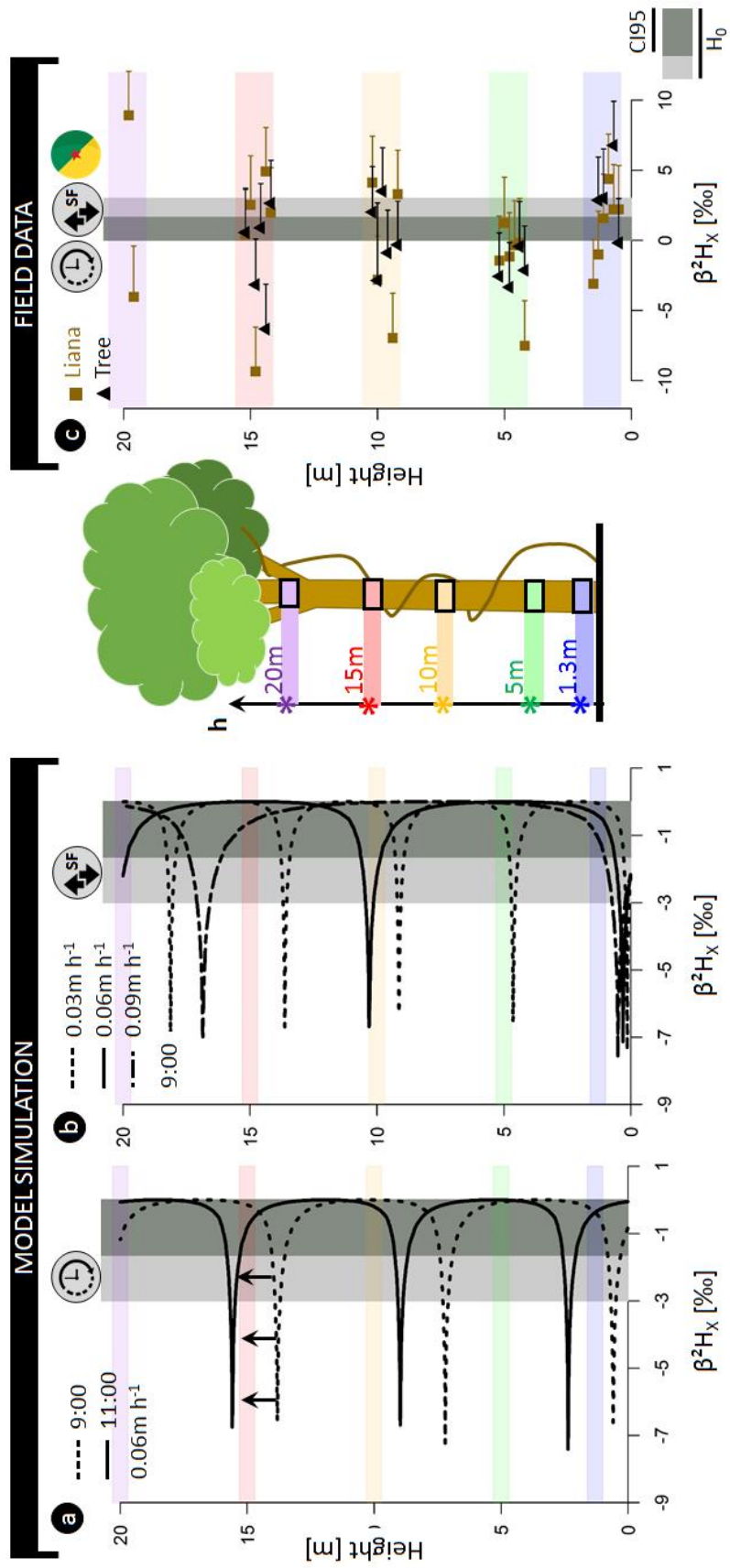
892

893 **Fig. 2. (a)** Schematic representation of the model and considered analysis detailed in the text.
894 **(b)** Simulated fluctuations in δ^2H composition of plant xylem water as a function of the
895 cumulative sap flow volume measured at various heights: stem base (0 m, black dashed), 1.3 m
896 (blue), 5 m (green) and 10 m (red). The horizontal grey colored envelope delineates the
897 acceptable variance from the stem mean according to the null model (H_0), i.e. assuming no
898 variance along the length of a lignified plant aside from potential extraction error (i.e. 3‰).
899 Herein, the dark grey envelope indicates the confidence interval comprising 95% of potential
900 extraction error (CI95).

901

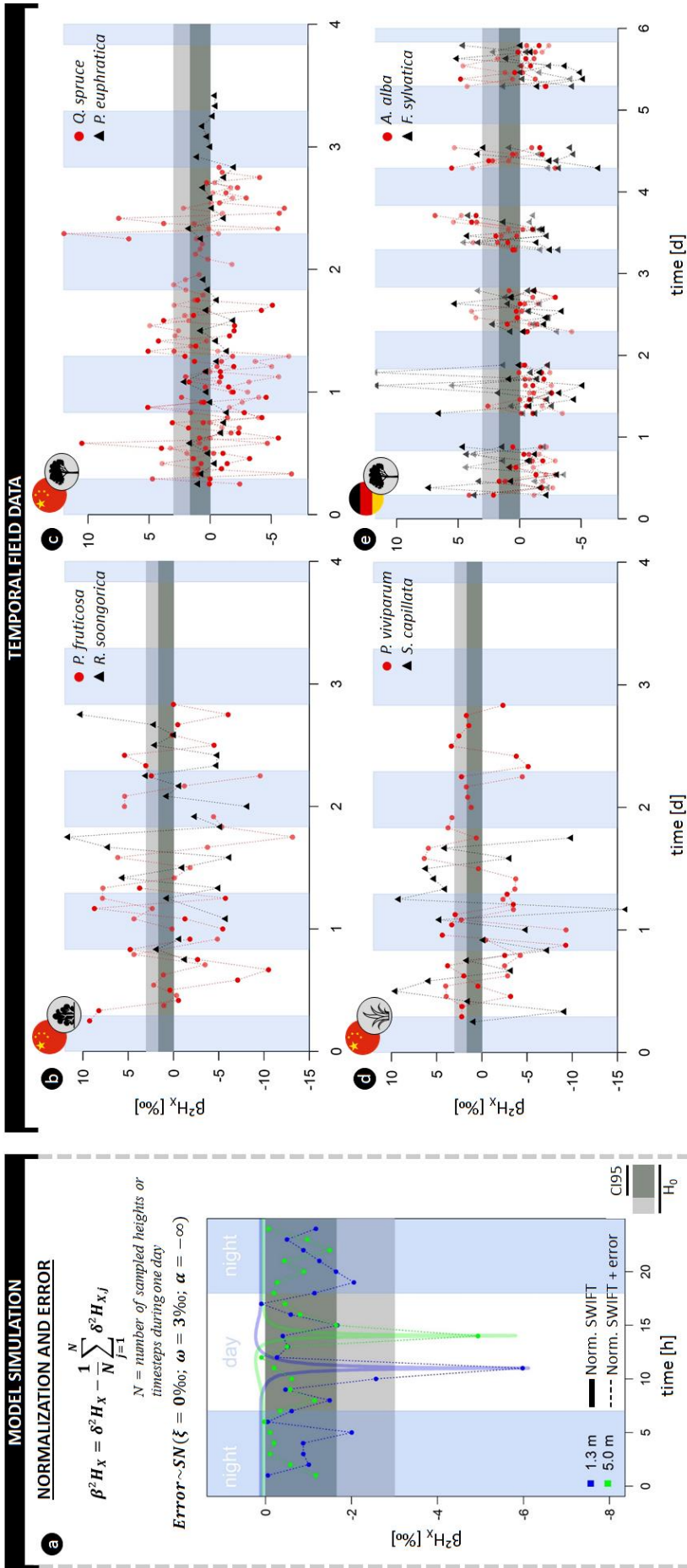
902

903



904 **Fig 3. (a)** Model outputs for model analysis A3 representing the normalized $\delta^2\text{H}$ composition
905 of xylem water ($\beta^2\text{H}_\text{X}$) as a function of the tree height simulated for different sampling times
906 (9:00 and 11:00). The modeled tree has an average daily sap flux density of 0.06 m h^{-1} (SF_s ; \sim
907 daily true sap flux density $SF_v = 0.42 \text{ m h}^{-1}$). **(b)** Model outputs for model analysis B where
908 $\beta^2\text{H}_\text{X}$ in relation to stem height is shown at 9:00 a.m., but parameterized with distinct SF_s , i.e.
909 $0.09, 0.06$ and 0.03 m h^{-1} (corresponding to SF_v of $0.64, 0.42$ and 0.19 m h^{-1} , respectively). The
910 standard parameterization used for both study analysis is detailed in Table S1. **(c)** Field
911 measurements of $\beta^2\text{H}_\text{X}$ for six lianas (■) and six trees (▲). Error whiskers are the combination
912 of potential extraction and measurement errors of the isotope analyzer. A species-specific
913 breakdown of the field data is provided in Fig S2. The horizontal grey colored envelope in all
914 panels delineates the acceptable variance from the stem mean according to the null model (H_0),
915 i.e. assuming no variance along the length of a lignified plant aside from potential extraction
916 error (i.e. 3%). Herein, the dark grey envelope indicates the confidence interval comprising
917 95% of potential extraction error (CI95).

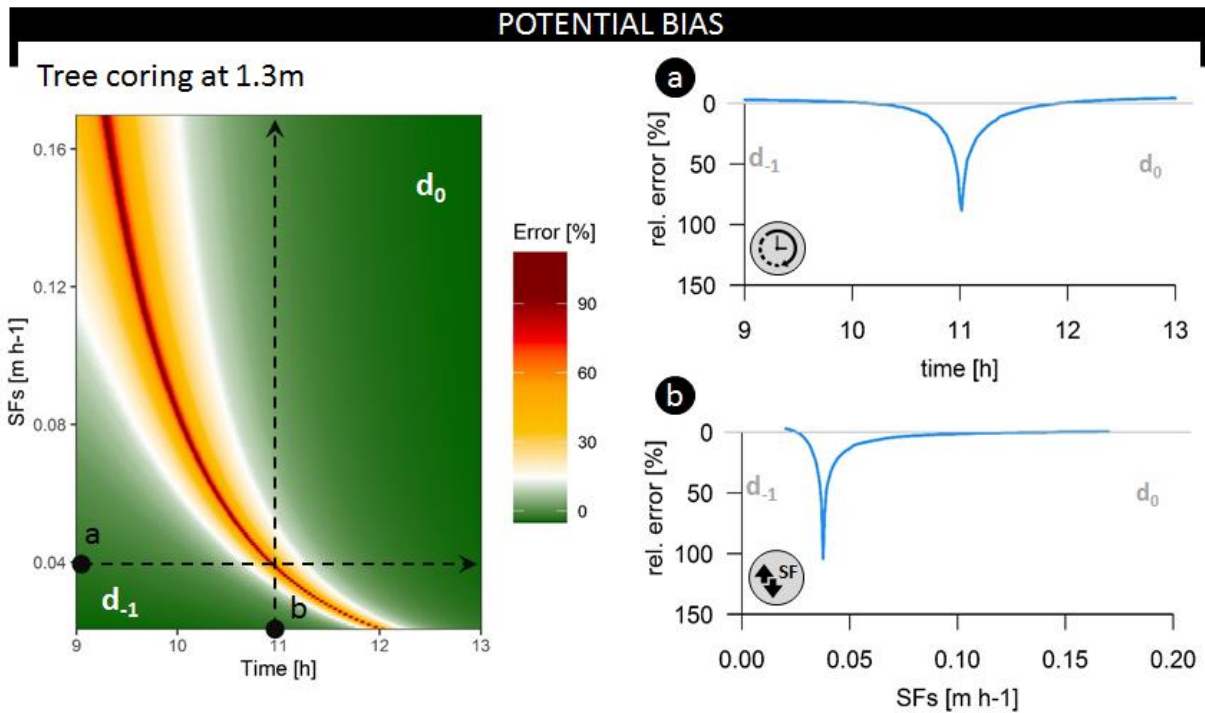
918



920 **Fig 4. (a)** Illustrative example of model simulations transformed in normalized $\delta^2\text{H}$ composition
921 of xylem water ($\beta^2\text{H}_X$) at 1.3 (blue) and 5m (green) sampling height, with the formula provided.
922 Thicker lines indicate model simulations without error, line connected dots indicate a scenario
923 of hourly sampling with consideration of extraction error (i.e. a negative skew-normal
924 distribution; $\zeta = 0\text{‰}$, the scale $\omega = 3\text{‰}$, and shape $\alpha = -\infty$). **(b-e)** High temporal field
925 measurements of $\beta^2\text{H}_X$ of (b) two shrubs, (c) two trees, and (d) two herb species sampled in the
926 Heihe River Basin (northwestern China); and (e) two tree species sampled in the “Freiamt”
927 field site in south-west Germany. The horizontal grey colored envelope in all panels delineates
928 the acceptable variance from the stem mean according to the null model (H_0), i.e. assuming no
929 variance along the length of a lignified plant aside from potential extraction error (i.e. 3‰).
930 Herein, the dark grey envelope indicates the confidence interval comprising 95% of potential
931 extraction error (CI95). A breakdown of the field data on species and individual level is
932 provided in the supplementary figures (Fig S3-S4-S5-S6)

933

934



935

936 **Fig 5.** Relative error on the inferred average root water uptake depth (i.e. bias between the

937 average daily and the instantaneous derived average RWU depth) at coring height of 1.3m,

938 throughout the common sampling period (9:00 until 13:00) and over a range of potential SF_s

939 (in m h^{-1}) – corresponding to SF_V range of $0.15\text{--}1.25 \text{ m h}^{-1}$. Both dotted lines describe test

940 scenarios evaluated in the breakup panels. The dynamics in relative error when sampling (a)

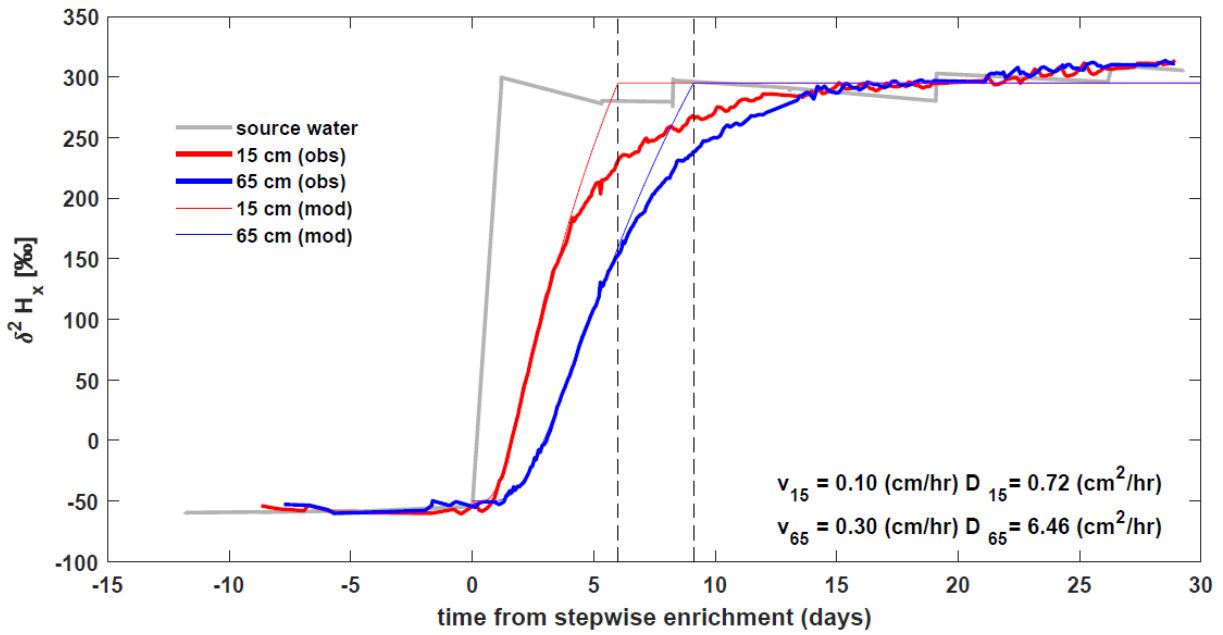
941 over different time steps, restricting sap flux density at 0.04 m h^{-1} (i.e. $SF_V = 0.28 \text{ m h}^{-1}$), or (b)

942 over different SF_s -values when restricting sampling time at 11 am. d_{-1} and d_0 indicate whether

943 the derived average RWU depth error corresponds to the previous or current day of

944 measurement.

945



946

947 **Fig. 6.** Basic model validation, comparing continuous *in situ* δ^2H_x measurements of a stepwise
 948 2H enrichment experiment (Marshall *et al.*, 2020) with analytical solutions of advection-
 949 diffusion equation, at heights 0.15m (—) and 0.65m (—) on a pine tree (*Pinus pinea* L). The
 950 source water of the intact-root, isotopic enrichment greenhouse experiment, is presented in
 951 grey. Model parameters, velocity, and diffusion were fitted by visual inspection independently
 952 for the two heights to match the initial increase in isotope signature (values reported in the
 953 bottom right)